Fast inertia-free volumetric light-sheet microscope

Journal:	*ACS Photonics*
Manuscript ID	ph-2017-00382g
Manuscript Type:	Letter
Date Submitted by the Author:	13-Apr-2017
Complete List of Authors:	Duocastella, Marti; Istituto Italiano di Tecnologia, Nanophysics Sancataldo, Giuseppe; Istituto Italiano di Tecnologia, Nanophysics Saggau, Peter; Allen Institute for Brain Science Ramoino, Paola; Universita degli Studi di Genova Scuola di Scienze Matematiche Fisiche e Naturali, DISTAV Bianchini, Paolo; Istituto Italiano di Tecnologia, Dept. of Nanophysics Diaspro, Alberto; Istituto Italiano di Tecnologia,

Fast inertia-free volumetric light-sheet microscope

Martí Duocastella[a]*, Giuseppe Sancataldo[a,b], Peter Saggau[c], Paola Ramoino[d], Paolo Banchini[a]*, Alberto Diaspro[a,e]

[a]Optical Nanoscopy, Nanophysics, Istituto Italiano di Tecnologia, Genova, Italy; [b]Dibris, Università di Genova, Italy; [c]Allen Institute for Brain Science, Seattle, Washington 98109, USA; [d]Dipteris Università di Genova, Italy. [e]Department of Physics, Università di Genova, Italy
*correspondence to: MD (marti.duocastella@iit.it) and PB (paolo.bianchini@iit.it)

Fast noninvasive three-dimensional (3D) imaging is crucial for the quantitative study of highly dynamic events ranging from flow cytometry to developmental biology. Light-sheet microscopy has emerged as the tool-of-choice for 3D characterization of rapidly evolving systems. However, to obtain a 3D image, either the sample or parts of the microscope are moved, limiting the acquisition speed. Here, we propose a novel inertia-free light-sheet-based scheme for fast volumetric imaging at unprecedented temporal resolution. Our approach comprises a novel combination of an acousto-optic-scanner to produce tailored illumination and an acoustic-optofluidic lens, placed in the detection path to generate an extended-depth-of-field. Such combination enables unsurpassed 3D imaging speeds up to 200 Volumes-per-Second. The volumetric acquisition speed is limited only by the acquisition frame rate of the camera and the desired signal-to-noise ratio. Our volumetric microscope allows invariant acquisition along the detection axis avoiding extensive processing or complex deconvolution methods to restore image quality.

Keywords: light sheet microscopy, acouto-optic devices, three-dimensional microscopy, flow cytometry

A key challenge in modern microscopy is to increase the acquisition rate of three-dimensional (3D) imaging from living systems or fast moving objects. Critical for fast 3D imaging is the capability to achieve optical sectioning, i.e. retrieving signal from a single focal plane of interest, at high spatiotemporal resolution. Within this framework, Light Sheet Microscopy (LSM) has recently been established as a suitable technique for 3D characterization of thick samples[1–6]. Indeed, compared to traditional 3D imaging methods, LSM shows intrinsic optical sectioning combined with a high signal-to-noise ratio (S/N), a low level of photo-toxicity, and a fast 2D wide-field acquisition scheme. The core concept of this technique lies in selective illumination of the sample with a sheet of light, created for instance by means of a cylindrical lens[7] or by a rapidly scanned Gaussian beam[8], placed at the focal plane of a perpendicularly oriented detection objective. In this optical configuration, only light from the plane of interest is collected by a wide-field detector, e.g. CMOS or CCD camera. It is worth noting that the illumination plane has to perfectly coincide with the detection plane, otherwise undesired blurring and image quality degradation will occur. Therefore, in order to ensure the overlap of light sheet and image plane, either the sample or microscope parts need to be synchronously moved. Even at imaging rates up to 50 volumes per second[9], the need for synchronization and mechanical translation limit the acquisition speed. This is particularly aggravating when high photon budgets are available (e.g. dark field imaging). Recently, alternative approaches have been proposed to overcome such requirements, disconnecting the

usual tradeoff between depth-of-field and spatial resolution inherent of traditional imaging systems. For instance, the detection path can be modified in order to produce an extended depth-of-field (EDOF), using wave-front coding[10,11] or introducing a flat dielectric material[12]. Although a significant increase in 3D imaging acquisition speed is obtained, these approaches require extensive post-processing or lack control of the EDOF extent. So far, only traditional light-sheet generation methods, using mechanical galvanometric scanners, have been combined with EDOF, resulting in an inertia-limited volumetric imaging rate of LSM.

Here we present a light-sheet microscope which obviates the use of any mechanical moving parts and allows for continuous volumetric imaging at unprecedented rates. Our strategy consists of coupling acousto-optic systems both in excitation and detection. We use an acoustic optical scanner (AOS) to create arbitrary shaped illumination patterns and an acoustic varifocal lens in the detection path to generate a dynamic EDOF without significant deterioration in lateral resolution (Fig. 1). The ability to create such arbitrary shaped illumination patterns gives us the flexibility to hop between different planes at high speed, or even restricting illumination to selected 2D regions of interest within the specimen. On the other hand the creation of a dynamic EDOF allows to directly produce a sharp image, without the need for complex deconvolution or image processing, for any given illumination plane placed within the EDOF of our microscope. Thus, we can quickly image extended volumes without mechanical sample translation. Note, in our inertia-free system, 3D volumetric acquisition speed is only limited by the integration time set on the camera and by the desired signal-to-noise ratio.

Principle of the inertia-free light-sheet microscope

The essence of the present light-sheet approach is the ability to dynamically extend the DOF of the detection objective while allowing axial translation of the light sheet without mechanical constrains, and thus at high speeds. To provide a description of the physical principle used to generate the tunable EDOF, we consider image formation in light-sheet microscopy to be given by the convolution product:

$$i(x,y,z) = s(x,y,z) * psf(x,y,z) \qquad (1)$$

where $i(x,y,z)$ is the resulting image intensity, $s(x,y,z)$ is the spatial distribution of sample and $psf(x,y,z)$ is the impulse response of the microscope or point spread function (PSF). Interestingly, by considering the light-sheet thickness uniform over the entire field-of-view, the PSF can be decoupled as the product of two distinct terms:

$$psf(x,y,z) = psf_{det}(x,y,z) \cdot ls(z) \qquad (2)$$

where $psf_{det}(x,y,z)$ is the point spread function of the detection system and $ls(z)$ is the axial intensity distribution of the light-sheet. $ls(z)$ is zero everywhere except in a small axial range given by the light-sheet thickness. This confined excitation intensity provides intrinsic optical sectioning: only light from the thin illuminated region contributes to image formation. Unfortunately, to avoid undesired blurring and degradation of image resolution, the illumination plane has to locate perfectly within the DOF of the detection objective. In other words, a sharp image is

obtained when the light-sheet intersects psf_{det} at its minimum lateral size. Ideally, to remove such constrains in the light-sheet positioning, one would like to have an elongated or needle-like $psf^*_{det}(x,y)$ with a lateral resolution independent of the z axis:

$$psf(x,y,z) = psf^*_{det}(x,y) \cdot ls(z) \qquad (3)$$

With such a system, sharp images could be acquired for any position of the illumination plane, while optical sectioning would be maintained with an axial resolution given by the light sheet thickness. A first approximation of such $psf^*_{det}(x,y)$ can be obtained by using very low-NA objective lenses, which have a large DOF and hence fulfill Eq. 3 throughout an extended axial range (e.g. 0.1 NA for 100 µm DOF). However, decreasing the NA comes at the cost of sacrificing lateral resolution. To circumvent this problem, we use an acousto-optic varifocal device (tunable acoustic gradient lens, TAG lens) that enables sinusoidal focus modulation at microsecond time scales. When combined with a microscope objective, the TAG lens behaves as a resonant axial scanner[13–15]. In this way, with a single camera snapshot (typical exposure time of milliseconds), an averaged image over multiple axial scans is captured, creating the effect of an EDOF without the need of camera/lens synchronization[16,17]. This effect had already been used in LSM to improve the uniformity of the illumination beam[18–20], but the unique benefits obtained when using the TAG lens in detection had not been reported. The effective detection $psf^*_{det}(\mathrm{x},\mathrm{y})$ can be considered as the incoherent superposition of instantaneous PSFs with different axial positions over the lens scanning range (Δz) [21], which yields to:

$$psf^*_{det}(\mathrm{x},\mathrm{y}) = \int_{\Delta \mathrm{z}} psf_{\mathrm{det}}(\mathrm{x},\mathrm{y},\mathrm{z})\mathrm{dz} \qquad (4)$$

This engineered PSF allows us to simultaneously capture multi-light-sheet data and thus volumetric images with near uniform lateral resolution within a range Δz. By using light-sheet illumination (Eq. 3), the essential ability to eliminate out-of-focus and scattered light from planes of non-interest is preserved. In order to rule out a potential loss in lateral resolution created by fast axial scanning we performed both simulations and experiments. Our tests demonstrated that, at conditions studied, no significant deterioration in lateral resolution is generated by our engineered PSF (see below). Therefore, our method provides a close to ideal PSF as described above: uniform high lateral resolution over an extended axial range, which makes it possible to remove the confocality requirement between detection and illumination planes of traditional LSMs.

Results

Initially, we validated our approach both theoretically and experimentally by calculating and measuring the EDOF accessible range with the microscope. To this end, we first simulated the point spread function of a detection objective (NA=0.3, wavelength 570 nm, refractive index 1.33) with and without the TAG lens. In particular, we used the Born and Wolf 3D optical model (*PSF generator ImageJ*) [22] to calculate the standard PSF of the detection system (Fig.2a, TAG OFF). The intensity profile of the simulated PSF along the axial and lateral directions (black lines) shows a fast decay in intensity and broadening of the PSF when moving away from the focal point. Under these conditions, the DOF was 12 µm. To simulate the EDOF obtained when the TAG lens is ON, we computed the effective PSF of the

system as the incoherent superposition of the previously obtained PSF at different axial positions. In more detail, we convolved the standard PSF with a line representing the overall scanning range (150 µm in the present case, above a factor 10 longer than the DOF of the native objective), as calculated from[23]. In Fig.2a (TAG ON), the simulated extended PSF presents a near uniform axial profile over an extension of 150 µm and a rapid decay (red lines). Importantly, the lateral extent of the PSF, and consequently the lateral resolution, is also maintained within this range. In fact, the lateral size of the PSF, in terms of full with at half maximum (FWHM), is 1.01 µm, practically identical with the in-focus PSF obtained at conditions of TAG lens OFF (0.98 µm). We repeated the above simulations for different NA objectives. In all cases, the change in the FWHM of the native in-focus PSF when generating the dynamic EDOF was below 5% (Table 1). Note, though, that the EDOF PSF obtained with the TAG lens is slightly wider at the base. Thus, depending on the S/N conditions, deconvolution is required to restore image quality. However, in contrast to other methods for extending the depth-of-field that can result in image artifacts during deconvolution[24], the space-invariant and nearly depth-invariant PSF greatly facilitates this operation. Indeed, the application of simple deconvolution algorithms, such as Wiener filters, suffices to achieve this[25]. Hence, the TAG lens enables a near uniform optical response of the detection system with invariant lateral resolution over a large extended axial range, without significant deterioration of the native resolution of the system. These characteristics are crucial for fast volumetric image acquisition in LSM, since they allow for linear depth-invariant imaging and obviate the need for extensive processing methods to restore image quality.

An experimental characterization of the EDOF capabilities of our system is presented in Fig.2b. In this case, we acquired images of sub-resolved static fluorescent beads (100 nm) embedded in agar gel with the TAG lens OFF and with the TAG lens operating at 100% of its driving voltage range and at a frequency of 144 kHz. Images were obtained by optically scanning the light-sheet through the sample along the axial direction in steps of 500 nm and maintaining the detection objective at a fixed position. A first glance at the XZ maximum intensity projections captured with TAG lens ON and TAG lens OFF clearly revealed a significant difference in the DOF. Indeed, in very good agreement with simulations, the axial range over which beads could be detected dramatically increases when using the TAG lens, (Fig.2b). The cumulative intensity profile along the Z direction can be used to quantify such enhancement in DOF, which in the performed experiment was a factor of 10. Moreover, the lateral profile of the EDOF PSF does not show important differences with respect to the native in-focus PSF. In fact, at conditions herein, image deconvolution was not required to restore image quality. A more detailed quantification of the effects of the time-averaged EDOF on the spatial resolving performance of the microscope is shown in Fig. 2c. In this case, we measured the microscope PSF as the FWHM of lateral and axial intensity profiles of isolated sub-diffraction fluorescent beads at different axial positions within the sample. Throughout the whole imaged volume, the measured PSFs remain approximately constant, with variations within the experimental error. As our results indicate, the fast varifocal lens system combined with selective plane illumination provides a space-shift-invariant PSF, comparable to that of the diffraction-limited PSF while covering a far larger region of focus. This makes 3D image acquisition possible by simply scanning the light-sheet along the z axis, while maintaining sample and objective lens in fixed positions.

One distinctive feature of our microscope is the capability to create a tunable DOF by simply changing the driving voltage amplitude applied to the varifocal lens. To evaluate the control of EDOF accessible by our system, we imaged an agar sample containing fluorescent beads at different driving amplitudes of the TAG lens. For each condition, we scanned the light-sheet over an axial distance of 300 um. The XZ maximum intensity projections, displayed in Fig.2d,

clearly show an increase in volumetric acquisition, and hence an extended DOF, with higher TAG lens driving voltages. In particular, there is a linear relationship between the amplitude of the driving voltage and the EDOF. In this way, by adjusting the driving voltage amplitude of the TAG lens, it is possible to achieve a tunable EDOF up to 10 times larger than the standard objective depth-of-field. Due to this unique feature, the EDOF can be adapted and optimized to sample geometry and volumetric extension.

As a proof-of-principle to demonstrate the fast imaging performance of our microscope, we imaged the flowing motion of beads (size 500 nm) in a defined detection volume. Note that imaging of fast moving sub-micrometer particles is of primary importance in several areas such as fluid mechanics, particle tracking, and flow cytometry. Since volumetric acquisition speeds are limited by the camera frame rate and by the defined axial extension, we assessed the capabilities of our microscope to perform volumetric measurements in various settings. First, we tested the suitability of our microscope for fast fluorescence imaging at two different volume extensions. Visualization 1 and 2 show flowing beads acquired at 45 volumes/second (axial range 70 µm) and 100 volumes/second (axial range 40 µm), respectively. In both cases, the size of a voxel, namely a tridimensional pixel, was ~0.27x0.27x2.4 μm^3. The frame rate of the sCMOS camera (Andor NEO 5.5) was set to 1,600 frames/second and 2,100 frames/second, respectively. Under these experimental conditions, the acquisition rate is mainly limited by the tradeoff between the active area of the camera and the relative maximum frame rate.

To further demonstrate the potential of our microscope system for fast imaging, we tracked the flowing motion of beads by using an ultrafast camera (PCO dimax.HS4). Here, instead of imaging by collecting fluorescence we used the scattering signal from the beads, i.e. in dark-field mode. An important characteristic of LSM is the possibility to operate with dark-field illumination (ultramicroscope) [16], and thereby only scattered light from the plane of interest contributes to the image formation. The resulting 3D trajectories of the moving beads and the dynamic evolutions are shown in Fig. 3 and in Visualization 3 and 4 respectively. For this imaging protocol, the CMOS camera frame rate was 10,000 frames/second (exposure time 91 µs/frame), each 3D stack covered 100 microns of axial extend (50 planes/volume), 110 microns of lateral extend and the acquisition took 5 ms. In this way, we reached an imaging speed of 200 Volumes per second. Considering the voxel size to be ~0.45x0.45x2.4 μm^3, our microscope can reach an imaging throughput of ~5.10^8 voxels/second.

Finally we showed the suitability of our light-sheet microscope for fast in vivo imaging of biological systems. For this purpose, we imaged the movements of a living single-cell microorganism (*Paramecium primaurelia*) at 11 volumes per second over an axial extension of 60 µm. Specimen was stained with a lipid dye (Nile Red, Molecular Probes) and embedded in low density agar gel. Fig. 4 shows the volumetric visualization and 3D maximum intensity projection of a time-lapse series encompassing 109 time points (exposure time 3 ms/frame, 30 planes/volume, 11 volumes/sec). Full spatial movements of a *Paramecium* were reconstructed in Visualization 5, with an overall resolution of 1 µm in xy and 2.4 µm in z.

Discussion

The present inertia-free light-sheet microscope provides unrivaled volumetric imaging speed, mainly limited by the frame rate of the camera and the S/N. Whereas technological developments of novel camera detectors show a continuous trend toward higher acquisition frame rates, the foreseen practical limit of our approach is the amount of photons that can be collected with respect to background or noise. Within this context, the evaluation of the photon

collection efficiency of our microscope is key. To this end, we simulated the EDOF PSF for different axial scanning ranges, following the procedure described above (NA=0.3, λ=500nm). We considered an average number of 8,000 collected photons per plane, and an average background of 130 photons per pixel (values obtained from experimental measurements using 500 nm beads and an exposure time of 100 µs). We computed the signal-to-background (S/B) as the maximum of the PSF divided by background noise. Note that, at low light levels, background noise dominates over other sources of noise, such as shot noise[26]. A plot of the S/B calculated for different z-scanning ranges, normalized by the value obtained for the native system PSF (TAG OFF), is presented in Fig. 5a. As expected, by increasing the axial scanning range, the S/B away from the original focus (0 µm position) increases, and so does the uniformity in S/B along the scanned range. This comes at the cost of a significantly reduced overall value of S/B with respect to the TAG OFF case. Because our extension in DOF is based on superimposing in-focus and out-of-focus PSFs, the longer the z-scanning range, the less significant the in-focus contributes become. To put our results in perspective, we compared the S/B of our method with arguably the most widely used strategy to generate an EDOF, namely wave-front coding with a cubic phase mask (CPM)[27]. In this case, we simulated the PSF generated using a CPM at the same conditions as described above, with a phase given by $\Psi = \exp(i2\pi\alpha(x^3+y^3))$, where α is the phase strength. By changing the value of α, it is possible to change the extension in DOF which we defined as the axial range where S/B decreases by a factor of 2. Fig. 5b presents the comparison between the two methods. Notably, the behavior in both cases is very similar, with the z-scanning approach presenting a slightly superior S/B throughout the whole range. Even if the differences between strategies are not compelling, in practice our approach has two main advantages. First, it is easy to implement and possible to restore the native system PSF by simply switching off the TAG lens. Second, our method is inherently tunable. In contrast, to achieve tunability of the axial range with a CPM, the use of spatial light modulators or other diffractive elements is required, which further reduces photon collection efficiency.

Based on the results from Fig. 5, our current strategy will perform best in cases with large photon availability, such as dark-field imaging. Instead, in the case of a restricted photon budget, our method will only be able to perform fast imaging over short axial ranges. Still, its imaging speed cannot be matched by the synchronous translation of light sheet and detection objective. Indeed, to achieve the volumetric imaging speed reported in this paper (200 volumes per second, exposure time of ~90 µs), light sheet and detection focal plane should synchronously move at a time scale clearly below 100 µs. Even if AODs placed in the illumination arm can reach this speed, to our knowledge, there are no high aperture systems capable of non-resonant focus translation with a response time below 100 µs that would be suitable for the detection.

Conclusion

The presented light-sheet microscope design absent of any mechanical moving parts can be used to significantly increase volumetric acquisition speed. Utilizing an unsynchronized acousto-optic varifocal lens in the detection path provides an extended depth-of-field while maintaining high lateral resolution. Thus, captured raw images can be directly used for 3D imaging without complex deconvolution or additional post-processing. When combined with acousto-optic deflectors to rapidly generate engineered illumination patterns, volumetric imaging speed becomes only limited by the desired signal-to-noise ratio and the camera acquisition frame rate. As our results demonstrate, unrivaled imaging speeds of up to 200 volumes per second are possible at diffraction-limited resolution. With faster and more sensitive cameras emerging, we anticipate that our inertia-free light-sheet microscope design will lead to

high-resolution 3D imaging at even higher volume rates, offering researches a unique tool to explore fundamental processes in science with an unprecedented temporal detail.

Methods

Microscope setup: A 488 nm beam from a CW laser (Coherent Sapphire) was expanded and directed to a 2D high-speed Acousto-Optic scanning system (Fig. 1). The laser power used in all experiments was 20 mW (measured after the objective). A scanning lens (200 mm) placed in front of the acousto-optic scanner (AOS) converted the angular deflection into a lateral displacement of the incident light. The beam was then directed by the excitation tube lens (200 mm) to the pupil of a low-NA illumination objective lens (Nikon 10X, NA 0.3). The sample, embedded in a cylinder of 1% agarose gel, was immersed in a water-filled chamber. Fluorescence emitted from the selectively illuminated plane was collected by the detection objective (Leica 20X, NA 0.5) orthogonally oriented to the illumination objective. Two lenses with equal focal length (100 mm) were placed in a 4f-configuration between the detection objective and the TAG lens (TAG lens 2.0, TAG Optics Inc.) to relay the back focal plane of the objective to the TAG lens position. The tube lens (240 mm) created an image of the illuminated sample plane on a CMOS camera, either an Andor NEO 5.5 (pixel size 6.5 µm) or a PCO dimax.HS4 (pixel size 11 µm). The latter had a built-in-memory of 18 GB which enabled recording data at 10,000 frames/s for time intervals of 5 seconds. A dichroic mirror (Chroma, Laser Beamsplitter zt 491 RDCXT) rejected excitation light and a band pass filter (Semrock, RazorEdge LP Edge Filter 488 LP) selected the captured fluorescence wavelength range. Due to the limited effective aperture of the TAG lens model used, our detection objective was restricted to NA = 0.3. Note that a TAG lens with a larger diameter could solve this problem. All data was processed using MATLAB and the NIS-Elements software.

AOS system. The acousto-optic scanner consisted of two acousto-optic deflectors (AOD) (IntraAction, ATD-7010CD2), one to scan the beam along the y axis, and thus generate the light sheet (AOD-Y) and one to translate the light sheet along the z axis (AOD-Z). Each AOD enabled a deflection angle up to 40 mrad with an efficiency of ~50%, thus ~25% of the power from the laser source was sent to the sample. The frequency of the AOD-Y was modulated at 10 kHz (the scanning period to generate the light sheet was 100 µs) when using the Andor camera, and at 25 kHz (scanning period of 40 µs) when using the PCO camera. The driving conditions for the AOD-Z were selected based on the particular exposure time of the camera, so that a single image frame corresponded to a fixed axial position. The linearity and accuracy of the AOD-Z system was characterized by using 500 nm beads translated with a nano-positioning system (Physic Instrumente, M-116). As the results demonstrate, the AOD-Z driving frequency is highly linear with the axial position of the light sheet within a range of ~100 µm, while preserving an accuracy better than 500 nm. Therefore, the driving frequency of the AOD-Z could be directly used to assign the axial location for each image plane.

Sample preparation*: Paramecium primaurelia* stock 90 was grown at 25°C in lettuce medium (pH 6.9) bacterized with *Enterobacter aerogenes*. Cells were harvested in the mid-log phase of growth. Paramecia were incubated with nile red (Molecular Probes, Invitrogen, Waltham, MA USA) at a final concentration of 4 µg/ml (prepared from a stock solution of 1 mg/ml in acetone) for 30 min in the dark at room temperature (23°C), and excess dye was removed by a brief rinsing in unbacterized culture medium.

Supplementary information

Visualization 1 and 2: flowing of 500 nm fluorescent beads captured at 45 volumes/second and 100 volumes/second over an axial range of 70 µm and 40 µm, respectively.

Visualization 3: imaging at 200 volumes/second (~5.10^8 voxels/second) of scattering beads flowing in a microchannel.

Visualization 4: temporal evolution of the tracked trajectories corresponding to Visualization 3.

Visualization 5: volumetric imaging of a living Paramecium at 11 volumes/second.

Author contributions

MD and GS contributed equally to this work.

Notes

The authors declare no financial competing interest.

Acknowledgements

The authors acknowledge financial support from Fondazione Istituto Italiano di Tecnologia and Nikon Imaging Center at the Fondazione Istituto Italiano di Tecnologia. The authors thank Luitpold Kaspar and Gerhard Holst from PCO AG for technical support. M.D. also acknowledges support from Compagnia di San Paolo SIME 2015-0682.

References

(1) Huisken, J.; Swoger, J.; Bene, F. Del; Wittbrodt, J.; Stelzer, E. H. K. Optical Sectioning Deep Inside Live Embryos by Selective Plane Illumination Microscopy. *Science (80-.).* **2004**, *305*, 1007–1009.

(2) Dodt, H.-U.; Leischner, U.; Schierloh, A.; Jährling, N.; Mauch, C. P.; Deininger, K.; Deussing, J. M.; Eder, M.; Zieglgänsberger, W.; Becker, K. Ultramicroscopy: Three-Dimensional Visualization of Neuronal Networks in the Whole Mouse Brain. *Nat. Methods* **2007**, *4*, 331–336.

(3) Cella, Z. F.; Lavagnino, Z.; Perrone, D. M.; Del, B. A.; Furia, L.; Faretta, M.; Diaspro, A. Live-Cell 3D Super-Resolution Imaging in Thick Biological Samples. *Nat.Methods* **2011**, *8*, 1047–1049.

(4) Mondal, P. P.; Diaspro, A. Simultaneous Multilayer Scanning and Detection for Multiphoton Fluorescence Microscopy. *Sci. Rep.* **2011**, *1*, 1–6.

(5) Vettenburg, T.; Corral, A.; Rodríguez-Pulido, A.; Flors, C.; Ripoll, J. Photoswitching-Enabled Contrast Enhancement in Light Sheet Fluorescence Microscopy. *ACS Photonics* **2017**, *4*, 424–428.

(6) Andilla, J.; Jorand, R.; Olarte, O. E.; Dufour, A. C.; Cazales, M.; Montagner, Y. L. E.; Ceolato, R.; Riviere, N.; Olivo-Marin, J.-C.; Loza-Alvarez, P.; *et al.* Imaging Tissue-Mimic with Light Sheet Microscopy: A Comparative Guideline. *Sci. Rep.* **2017**, *7*, 44939.

(7) Huisken, J.; Swoger, J.; Bene, F. Del; Wittbrodt, J.; Stelzer, E. H. K. Live Embryos by Selective Plane Illumination Microscopy. *Science (80-.).* **2004**, *305*, 1007–1009.

(8) Keller, P. J.; Schmidt, A. D.; Santella, A.; Khairy, K.; Bao, Z.; Wittbrodt, J.; Stelzer, E. H. K. Fast, High-Contrast Imaging of Animal Development with Scanned Light Sheet-Based Structured-Illumination Microscopy. *Nat. Methods* **2010**, *7*, 637–642.

(9) Fahrbach, F. O.; Voigt, F. F.; Schmid, B.; Helmchen, F.; Huisken, J. Rapid 3D Light-Sheet Microscopy with a Tunable Lens. *Opt. Express* **2013**, *21*, 21010–21026.

(10) Olarte, O. E.; Andilla, J.; Artigas, D.; Loza-Alvarez, P. Decoupled Illumination Detection in Light Sheet Microscopy for Fast Volumetric Imaging. *Optica* **2015**, *2*, 702.

(11) Quirin, S.; Vladimirov, N.; Yang, C.-T.; Peterka, D. S.; Yuste, R.; Ahrens, M. Calcium Imaging of Neural Circuits with Extended Depth-of-Field Light-Sheet Microscopy. *Opt. Lett.* **2016**, *41*, 855.

(12) Tomer, R.; Lovett-barron, M.; Kauvar, I.; Broxton, M.; Deisseroth, K. Resource SPED Light Sheet Microscopy : Fast Mapping of Biological System Structure and Function. *Cell* **2015**, *163*, 1796–1806.

(13) Duocastella, M.; Arnold, C. B. Enhanced Depth of Field Laser Processing Using an Ultra-High-Speed Axial Scanner. *Appl. Phys. Lett.* **2013**, *102*, 2011–2015.

(14) Duocastella, M.; Vicidomini, G.; Diaspro, A. Simultaneous Multiplane Confocal Microscopy Using Acoustic

Tunable Lenses. *Opt. Express* **2014**, *22*, 19293.
(15) Duocastella, M.; Theriault, C.; Arnold, C. B. Three-Dimensional Particle Tracking via Tunable Color-Encoded Multiplexing. *Opt. Lett.* **2016**, *41*.
(16) Liu, S.; Hua, H. Extended Depth-of-Field Microscopic Imaging with a Variable Focus Microscope Objective. *Opt. Express* **2011**, *19*, 353–362.
(17) Sancataldo, G.; Scipioni, L.; Ravasenga, T.; Lanzanò, L.; Diaspro, A.; Barberis, A.; Duocastella, M. Three-Dimensional Multiple-Particle Tracking with Nanometric Precision over Tunable Axial Ranges. *Optica* **2017**, *4*, 367.
(18) Dean, K. M.; Fiolka, R. Uniform and Scalable Light-Sheets Generated by Extended Focusing. *Opt. Express* **2014**, *22*, 26141.
(19) Duocastella, M.; Arnold, C. B.; Puchalla, J. Selectable Light-Sheet Uniformity Using Tuned Axial Scanning. *Microsc. Res. Tech.* **2016**, 1–10.
(20) Hedde, P. N.; Gratton, E. Selective Plane Illumination Microscopy with a Light Sheet of Uniform Thickness Formed by an Electrically Tunable Lens. *Microsc. Res. Tech.* **2016**.
(21) Olivier, N.; Mermillod-Blondin, A.; Arnold, C. B.; Beaurepaire, E. Two-Photon Microscopy with Simultaneous Standard and Extended Depth of Field Using a Tunable Acoustic Gradient-Index Lens. *Opt. Lett.* **2009**, *34*, 1684–1686.
(22) Kirshner, H.; Aguet, F.; Sage, D.; Unser, M. 3-D PSF Fitting for Fluorescence Microscopy: Implementation and Localization Application. *J. Microsc.* **2013**, *249*, 13–25.
(23) Duocastella, M.; Sun, B.; Arnold, C. B. Simultaneous Imaging of Multiple Focal Planes for Three-Dimensional Microscopy Using Ultra-High-Speed Adaptive Optics. *J Biomed Opt* **2012**, *17*, 50505.
(24) Demenikov, M.; Harvey, A. R. Image Artifacts in Hybrid Imaging Systems with a Cubic Phase Mask. *Opt. Express* **2010**, *18*, 8207–8212.
(25) Kuthirummal, S.; Nagahara, H.; Zhou, C.; Nayar, S. K. Flexible Depth of Field Photography. *IEEE Trans. Pattern Anal. Mach. Intell.* **2011**, *33*, 58–71.
(26) Thompson, R. E.; Larson, D. R.; Webb, W. W. Precise Nanometer Localization Analysis for Individual Fluorescent Probes. *Biophys. J.* **2002**, *82*, 2775–2783.
(27) Dowski, E. R.; Cathey, W. T. Extended Depth of Field through Wave-Front Coding. *Appl. Opt.* **1995**, *34*, 1859–1866.
(28) Martinez-Corral, M.; Hsieh, P.-Y.; Doblas, A.; Sanchez-Ortiga, E.; Saavedra, G.; Huang, Y.-P. Fast Axial-Scanning Widefield Microscopy with Constant Magnification and Resolution. *J. Disp. Technol.* **2015**, 1–1.

Tables

NA	Lateral PSF (nm)		Axial PSF (μm)		z-scan range
	TAG OFF	TAG ON	TAG OFF	TAG ON	
0.3	978	1013	15	113	100
0.5	586	610	5.4	51	50
0.7	420	440	2.7	28	27

Table 1. Comparison of the FWHM of the lateral and axial simulated PSFs for different NA objectives with the TAG lens OFF and ON. The z-scan range considered for the TAG ON case is indicated on the right column. Because spherical aberration can degrade lateral resolution at positions far away from the native focal plane[28], values for the z-scan range of only ~10 times the original axial PSF were considered.

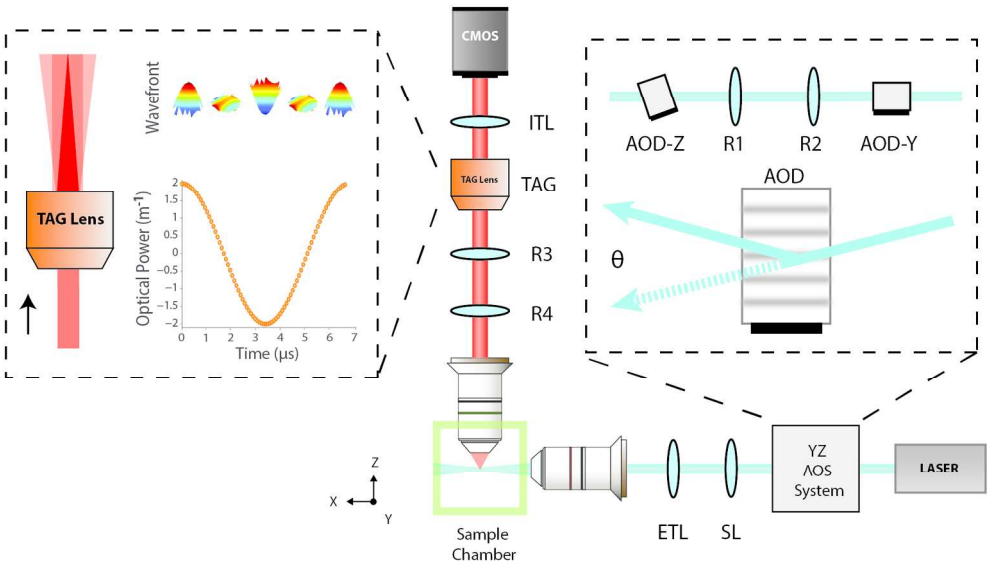

168x95mm (300 x 300 DPI)

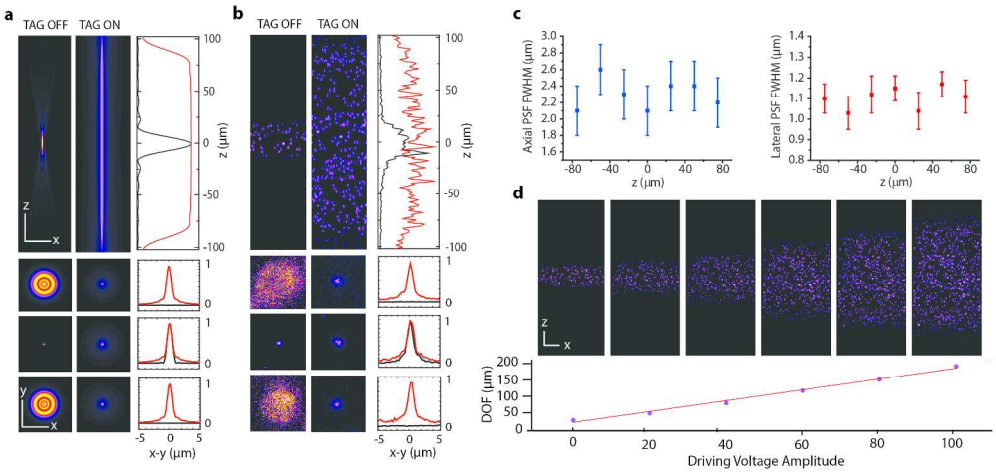

249x116mm (300 x 300 DPI)

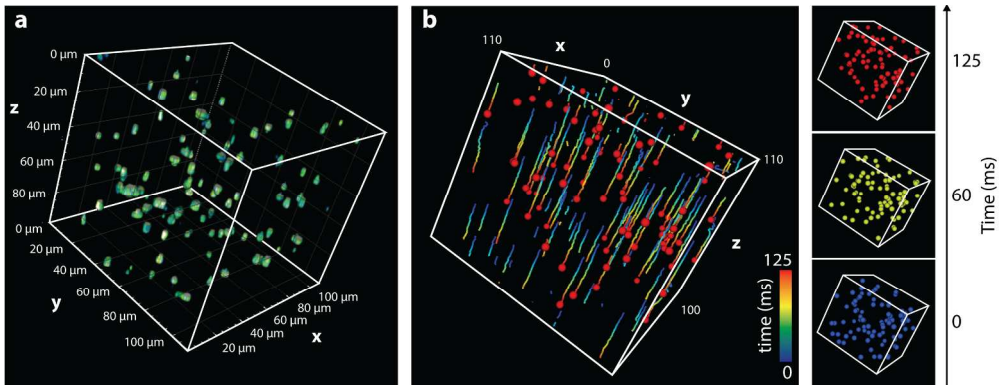

219x83mm (300 x 300 DPI)

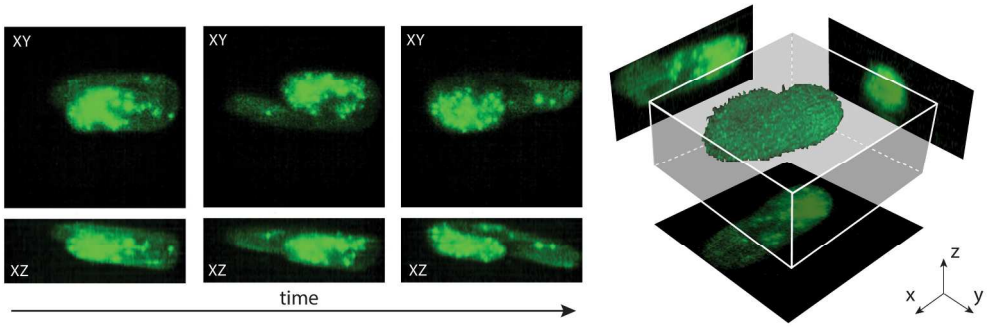

205x67mm (300 x 300 DPI)

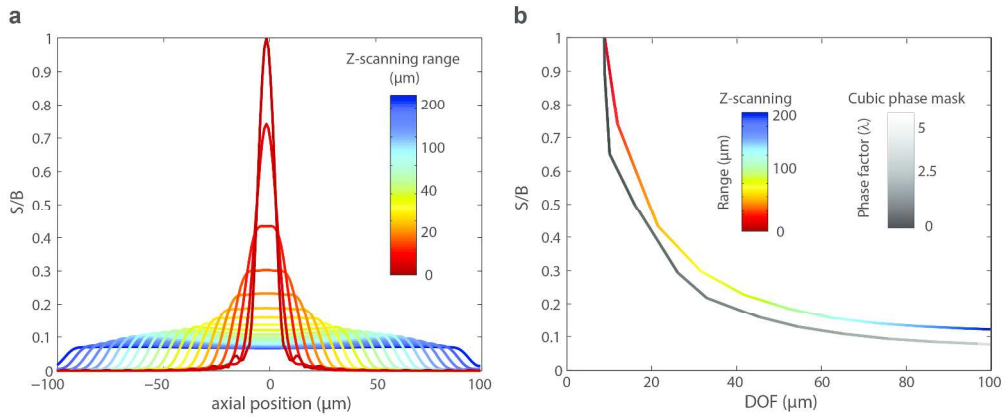

271x112mm (300 x 300 DPI)